



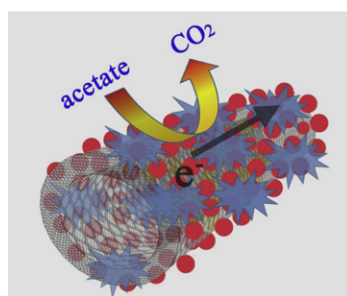
Short communication

TiO₂ nanoparticles-decorated carbon nanotubes for significantly improved bioelectricity generation in microbial fuel cellsZhenhai Wen^{a,1}, Suqin Ci^{a,b,c,1}, Shun Mao^a, Shumao Cui^a, Ganhua Lu^a, Kehan Yu^a, Shenglian Luo^c, Zhen He^{b,**}, Junhong Chen^{a,*}^a Department of Mechanical Engineering, University of Wisconsin-Milwaukee, 3200 North Cramer Street, Milwaukee, WI 53211, USA^b Department of Civil Engineering and Mechanics, University of Wisconsin-Milwaukee, 3200 North Cramer Street, Milwaukee, WI 53211, USA^c Key Laboratory of Jiangxi Province for Ecological Diagnosis-Remediation and Pollution Control, Nanchang Hangkong University, Nanchang 330063, China

H I G H L I G H T S

- A reliable method to synthesize TiO₂ nanoparticles-decorated CNTs.
- Large surface area, high electrical conductivity, good biocompatibility.
- Significantly improved MFC performance with CNTs@TiO₂ anode.
- Synergetic effects between TiO₂ and CNT are responsible for the improved performance.

G R A P H I C A L A B S T R A C T



A R T I C L E I N F O

Article history:

Received 28 December 2012

Received in revised form

23 January 2013

Accepted 24 January 2013

Available online 1 February 2013

Keywords:

Nanohybrid anode

TiO₂

Carbon nanotube

Microbial fuel cell

A B S T R A C T

A facile and reliable method has been developed to synthesize nanohybrids of anatase TiO₂ nanoparticles-decorating carbon nanotubes (CNTs@TiO₂). The nanohybrid displays a unique feature of having CNTs encapsulated inside and anatase TiO₂ nanoparticles coating on the CNT surface. Comprehensive characterizations suggest that CNTs@TiO₂ nanohybrids exhibit unique properties of CNTs and TiO₂ nanoparticles with one-dimensional structure, excellent electrical conductivity, high surface area, and good biocompatibility. The electrochemical properties of CNTs@TiO₂ nanohybrids were systematically investigated, it was revealed that the CNTs@TiO₂ nanohybrids showed great promise as anode materials of microbial fuel cells (MFCs). Compared with pure TiO₂ nanoparticles and CNTs alone, CNTs@TiO₂ nanohybrids exhibited a much higher output current, power density, and Coulombic efficiency when used as anode materials of MFCs. The as-developed synthetic route opens up a new avenue for designing CNTs-based nanohybrid materials for various applications benefiting from the synergetic effect among constituents.

© 2013 Elsevier B.V. All rights reserved.

1. Introduction

There have been great efforts into the development of microbial fuel cells (MFCs) because they are envisaged to be a promising wastewater treatment technology with direct recovery of electric energy. MFCs can potentially offer a sustainable power source with advantages of low maintenance, environmentally friendliness, high conversion efficiency, ambient and low operating temperature.

* Corresponding author. Tel.: +1 4142292615; fax: +1 4142296958.

** Corresponding author.

E-mail addresses: zhenhe@uwm.edu (Z. He), jhchen@uwm.edu (J. Chen).¹ These authors contributed equally to this work.

[1–4]. As bio-electrochemical systems, MFCs can directly convert chemical energy in organic compounds to electricity via microbial metabolism, in which inexpensive bacterial catalysts, essentially “free”, are used for catalyzing electrochemical oxidation of fuels, in sharp contrast to traditional fuel cells that indispensably use precious metal catalysts [5,6]. Although MFCs have been demonstrated since early 1900s, there is still much challenge to address existing issues of low current and low power density in MFCs [7,8].

It is well known that the performance of an MFC is highly dependent on the anode electrode, on which microbes are attached to catalyze the fuel oxidation for production of electrons and protons [9,10]. Therefore, one of the major objectives in the MFC research is to design and synthesize advanced electrode materials with a lower cost, increased efficiency, and improved durability. Ideal anode materials for MFCs should have good intrinsic biocompatibility (the quality of not having toxic effects on biological systems) for microbial inoculum, growth, and adhesion, and excellent conductivity for electron transfer. Other properties, such as long-term stability, large surface area, proper porous structure, and favorable surface modification, are also highly desirable [11,12]. Various carbon-based materials, including graphite brush, carbon nanotubes, and graphene, have recently attracted increasing research interest for utilization as anodes of MFCs [13–15]. However, the poor biocompatibility and limited active reaction sites of those carbon materials restrict biofilm formation and thus limit the resulting power density.

Titanium dioxide (TiO_2) stands as one of the most attractive metal oxides and has received extensive attention owing to its unique physical and chemical properties and various advantages such as abundance, low cost, and structural stability. As a result, TiO_2 has been applied in many fields including photocatalysis, sensors, solar cells, and lithium-ion batteries (LIBs) [16,17]. For instance, TiO_2 has been offering a lot of hope in easing the energy crisis through efficient utilization of solar energy within solar cells or water-splitting devices and addressing many serious environmental issues and pollution challenges based on its excellent photocatalytic properties [18–20]. It was previously reported that TiO_2 nanohybrids with polyaniline (PANI- TiO_2) can be used as anode electrodes of MFCs and significantly improve the power density in comparison to MFCs with carbon nanotube (CNT)-PANI composites or graphite/polytetrafluoroethylene (PTFE) [21–23]. However, the electrical conductivity in conductive polymer of PANI is not good enough to assist electron transfer from microbes to the current collector, and the long-term stability of PANI is also a major concern for its practical application in MFCs. Additionally, the power density delivered by a PANI- TiO_2 MFC is still quite low (1495 mW m^{-2}). On the other hand, CNTs have been widely investigated for fabricating hybrids for various potential applications thanks to their remarkable thermal, electronic, photonic, and unique structural features [24,25]. Based on these demonstrations, we are motivated to design and fabricate CNT- TiO_2 nanohybrids for the purpose of promoting the anode performance of MFCs. However, there is a lack of effective method to load well-dispersed TiO_2 nanoparticles on CNTs because of the inhomogeneity, hydrophobic nature, and inertness of CNT surfaces, and the difficulty in controlling growth of TiO_2 nanoparticles [26,27], not to mention their applications in MFC systems.

We recently demonstrated that CNTs-modified carbon cloth, when used as anode of MFCs, exhibited a significantly improved performance compared with bare carbon cloth in terms of output current density and output power density [28]. Herein, we report a reliable procedure to fabricate CNT- TiO_2 (CNTs@ TiO_2) nanohybrids with well-dispersed TiO_2 nanoparticles-decorating CNTs. Such hybrid nanostructures combine various advantages of CNTs and TiO_2 with excellent electrical conductivity, high surface area,

and good biocompatibility, which renders it as a promising electrode material for MFCs. To this end, the as-prepared CNTs@ TiO_2 nanohybrids were systematically investigated as anode electrodes for MFCs, and it was revealed that CNTs@ TiO_2 -based MFCs significantly outperform CNTs- or TiO_2 nanoparticles-based MFCs in terms of output current density and power density.

2. Experimental section

2.1. Materials and synthesis

CNTs (200 nm in diameter) were directly purchased from Carbon Nanotechnologies, Inc. All chemicals were purchased from Sigma Aldrich and used without further purification. The carbonaceous polymer-modified CNTs were prepared by a hydrothermal method. In a typical experiment, 0.1 g CNTs were added and dispersed in 40 mL glucose solution (0.5 mg mL^{-1}) with the assistance of sonication. The mixture was then transferred to a 100 mL teflon-lined stainless steel autoclave and placed in the oven with a temperature of 180°C for 5 h. The final precipitates (CNTs@C_{polymer}) were centrifuged, washed, and dried for further utilization. One gram of the dry products was then dispersed in 20 mL ethanol under sonication. Next, 2 mL of titanium isopropoxide (TIP, 97%) was added under vigorous agitation for 2 h. The obtained slurry was centrifuged and washed for three times with distilled absolute alcohol to remove the un-adsorbed Ti^{4+} . The products after drying were then annealed at 400°C under air atmosphere to decompose most of the carbonaceous polymer, with the resulting samples denoted as CNTs@ TiO_2 . The SnO_2 /CNTs nanohybrids were prepared using the similar procedure but with SnCl_4 as the source of Sn.

2.2. Characterization

The morphologies of the as-prepared samples, selected-area electron diffraction (SAED) pattern, and energy-dispersive X-ray spectrum were obtained using a Hitachi (H 9000 NAR) transmission electron microscope (TEM) and a Hitachi S-4800 scanning electron microscope (SEM) equipped with an energy-dispersive X-ray spectroscopy (EDX) analyzer. Powder X-ray diffraction (XRD) was performed on a Scintag XDS 2000 X-ray powder diffractometer with monochromatized CuK_α radiation ($\lambda = 1.5418 \text{ \AA}$); the data were collected between scattering angles (2θ) of 10° and 70° . X-ray photoelectron spectroscopy (XPS) was conducted using HP 5950A with an MgK_α as source and the C1s peak at 284.6 eV as an internal standard. Raman spectroscopy and Fourier transform infrared spectroscopy (FTIR) were conducted with a Renishaw Raman microscope and a Mattson Galaxy FTIR spectrometer, respectively. N_2 adsorption–desorption measurements were carried out at 77 K using a Quantachrome Autosorb gas-sorption system.

2.3. MFC construction and operation

The CNTs@ TiO_2 nanohybrids were mixed with 5% Nafion solution in an ultrasonic bath, and then deposited on both sides of carbon cloth ($1.5 \text{ cm} \times 3 \text{ cm}$) with a loading of $\sim 5 \text{ mg cm}^{-2}$. After drying at room temperature overnight, the modified electrodes were used as the anode in MFCs. The same procedure was used to prepare CNTs- and TiO_2 -based anodes. A batch-operated two-chamber MFC was constructed by connecting two glass bottles (liquid volume of 120 mL each) with cation exchange membrane (CEM, Membrane International, Inc.) as a separator. Three anodes including CNTs@ TiO_2 , CNTs, and TiO_2 , were installed into the same anode chamber without contact between each other and shared the same cathode (carbon brush, Gordon Brush Mfg. Co. Inc.,

Commerce, CA, USA). Such an arrangement could minimize the effect of the (different) cathode on experimental results.

The anolyte was prepared according to the previous report with sodium acetate (1.0 g L^{-1}) as an electron donor [28,29]. The aerobic/anaerobic sludge from a local wastewater treatment plant (South Shore, Milwaukee, WI, USA) was used as inocula in the anode compartment of the MFC. The cathode chamber was filled with $1.0 \text{ M K}_3[\text{Fe}(\text{CN})_6]$ as terminal electron acceptor in 100 mM phosphate buffer solution. Initial bacteria growth and biofilm development were induced using a $1.5 \text{ k}\Omega$ external resistance across the MFC until a relatively stable voltage output was obtained. For testing the Coulombic efficiency (CE) of each MFC, only the MFC to be measured was run under the same condition as described above and the other two anodes were disconnected.

2.4. MFC characterization

The cell voltage across the external circuit and the anode potential (vs. Ag/AgCl , 1.0 M KCl) were recorded every 5 min by a digital multimeter (2700, Keithley Instruments, Inc., Cleveland, OH). Polarization curves were obtained using a potentiostat (Reference 600, Gamry Instruments, Warminster, PA) with a scan rate of 0.6 mV s^{-1} . The maximum power/current density was calculated by normalizing the anode surface area. Coulombic efficiency (CE) was obtained by calculating the ratio of total recovered Coulombs by integrating the current over time to the theoretical amount of Coulombs that were determined from the amount of acetate consumed.

Electrochemical impedance spectroscopy (EIS) was employed to measure the MFC anode internal resistances, and the measurement was conducted using a potentiostat at the open circuit potential (V_{oc}) in a frequency of 100 kHz – 50 mHz with the anode as the working electrode, the cathode as the counter electrode, and Ag/AgCl (1.0 M KCl) electrode as the reference electrode. The EIS data were plotted in the form of Nyquist curve in which the Ohmic resistance (R_{Ω}) and charge-transfer resistance (R_{ct}) were determined by fitting the measured impedance data to an equivalent circuit.

3. Results and discussions

Fig. 1 schematically describes the entire process for preparing the TiO_2 nanoparticles-decorating CNTs nanohybrids. Firstly, a film of carbonaceous polymer was modified on the surface of CNTs through *in situ* glucose hydrothermal polymerization on the CNTs surface [30]. A large amount of Ti^{4+} can be adsorbed on the surface of the functionalized CNTs ($\text{CNTs@C}_{\text{polymer}}$) due to a large number of active groups on $\text{CNTs@C}_{\text{polymer}}$ [31,32]. The Ti^{4+} -adsorbing $\text{CNTs@C}_{\text{polymer}}$ was then annealed to achieve decomposition

of the carbonaceous polymer and simultaneously form TiO_2 nanoparticles-decorated CNTs (CNTs@TiO_2) hybrids. It should be noted that the synthesis strategy could be easily extended to prepare other metal oxide-modified CNTs nanohybrids. For instance, using the similar method, we have successfully prepared CNTs@SnO_2 nanohybrids, in which SnO_2 nanoparticles can be uniformly deposited on the CNTs surface (Supporting information, Fig. S1).

Scanning electron microscopy (SEM) and transmission electron microscopy (TEM) were utilized to characterize the morphologies of as-prepared CNTs@TiO_2 nanohybrids. Fig. 2a–c displays SEM images of the as-prepared CNTs@TiO_2 at different magnifications. A general morphology of the samples is shown in Fig. 2a, from which one can clearly observe the 1D nanostructures with lengths of a few microns and diameters of around 300 nm . The magnified SEM image, as shown in Fig. 2b, reveals that a large number of nanoparticles are uniformly anchored on the surface of CNTs, implying that TiO_2 nanoparticles were successfully deposited on the CNT surface. Fig. 2c presents a typical SEM image of the as-prepared CNTs@TiO_2 with end-on view, which confirms that the as-prepared hybrids possessed an open-end tubular structure with an inner diameter of around 200 nm . A TEM image of CNTs@TiO_2 is shown in Fig. 2d, which further confirms that TiO_2 nanoparticles are decorated on the surface of CNTs. Fig. 2e presents selected-area electron diffraction (SAED) patterns of CNTs@TiO_2 nanohybrids; several well-defined rings can be assigned to diffraction planes of anatase TiO_2 and CNTs, respectively. High-resolution TEM (HRTEM) images were taken to study the detailed crystalline structure of TiO_2 nanoparticles overlaying on CNTs (Fig. 2f–g). As indicated by the arrow, TiO_2 nanoparticles anchored on the CNTs are estimated to have an average diameter of 5 – 10 nm with a crystalline spacing of 0.35 nm corresponding with anatase (101) plane. In addition, one can observe that graphite crystalline spacing of 0.34 nm is orientated along the direction of the axis of CNTs. The CNTs@TiO_2 was further characterized by taking elemental mapping images to analyze the element distribution. The uniform distribution of Ti, C, and O elements in the samples further confirms that TiO_2 nanoparticles homogeneously decorate the CNT surface (Supporting information, Fig. S2). For comparison, TiO_2 nanoparticles with an average diameter of 50 nm were also prepared through a sol-gel method (Supporting information, Fig. S3).

Powder X-ray diffraction (XRD) was performed to study the crystallographic structure of the samples (Fig. 3a). The crystallinity of TiO_2 nanoparticles is evidenced by clear peaks corresponding with the anatase phase TiO_2 (JCPDS, No. 21-1272). All anatase peaks also appear in the CNTs@TiO_2 nanohybrids accompanying with typical CNT (002) peaks. No impurity peak was observed in both XRD patterns, implying the absence of amorphous, rutile, and brookite phases of TiO_2 . According to the Scherrer's formula, the

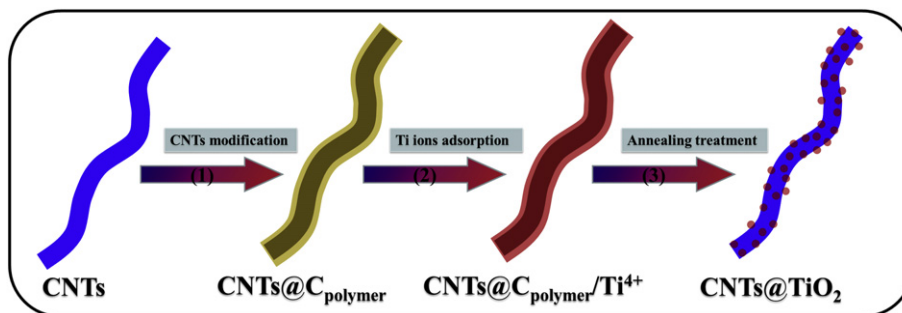


Fig. 1. Schematic illustration for the synthesis of CNTs@TiO_2 hybrids. (1) Hydrothermal growth of a carbonaceous polymer film on CNTs. (2) Adsorption of Ti^{4+} on $\text{CNTs@C}_{\text{polymer}}$. (3) Annealing at 400°C in air environment to decorate CNTs with TiO_2 nanoparticles.

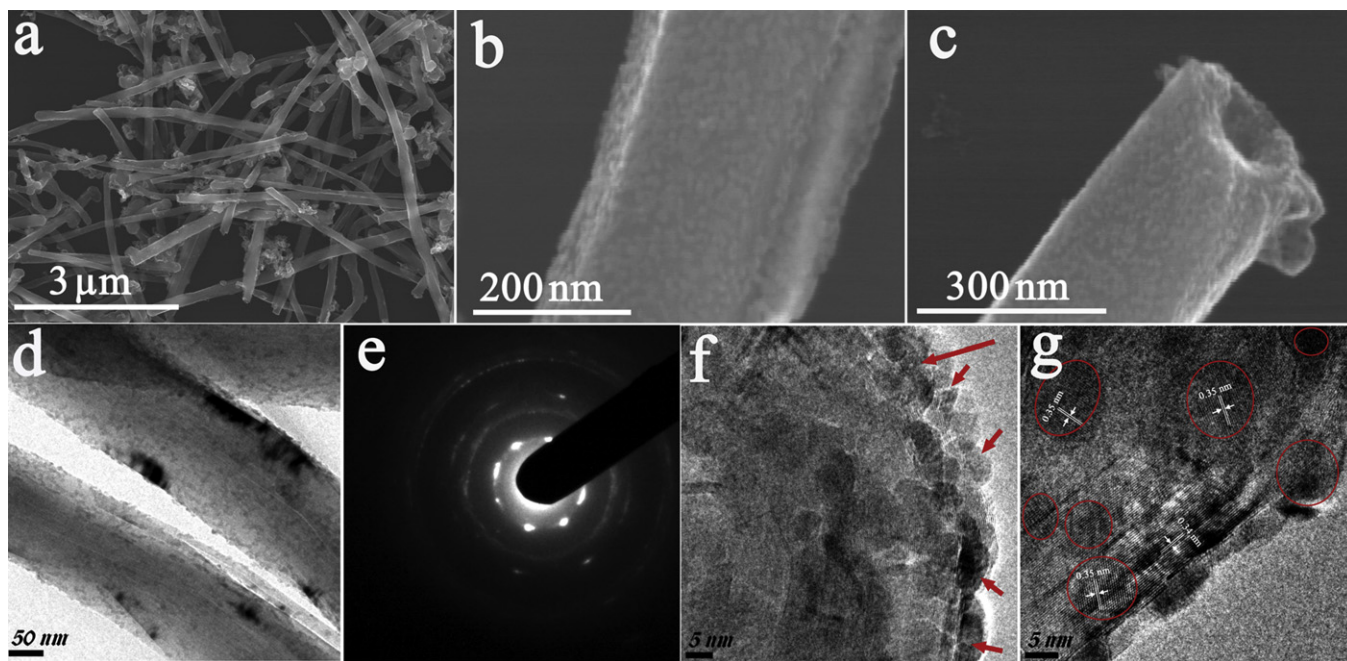


Fig. 2. SEM image of the CNTs@TiO₂ hybrid (a); magnified SEM images of the middle section (b) and top end (c) in a single CNTs@TiO₂ hybrid; TEM image (d) and SAED pattern (e) of CNTs@TiO₂; and HREM images of top end (f) and middle section (g) of a single CNTs@TiO₂ hybrid.

average size of TiO₂ nanoparticles is estimated as 6.9 nm based on the half peak width of the TiO₂ (200) peak, which is basically consistent with the HRTEM result.

Raman spectroscopy was conducted for further investigation of the chemical composition among the samples of CNTs@TiO₂ nanohybrids, CNTs, and pure phase TiO₂ nanoparticles, as shown in Fig. 3b. As expected, the CNTs@TiO₂ displays spectroscopic properties from both CNTs and TiO₂. Specifically, vibrational peaks at about 400, 515, and 639 cm⁻¹ in pure phase TiO₂ nanoparticles are well consistent with B_{1g}, A_{1g}, and E_g characteristic peaks of anatase TiO₂ [33]. These peaks also appear in CNTs@TiO₂ nanohybrids with remarkable broadening and negative shifting; such changes can be reasonably attributed to the interaction between TiO₂ and CNTs. Additionally, three peaks can be observed in the CNTs@TiO₂ nanohybrids at about 1330, 1568 and 1586 cm⁻¹, which can be assigned to the D, G⁻, and G⁺ peaks of CNTs [34]. These peaks also show evident difference in peak position and peak intensity in comparison with pure CNTs, further confirming the interaction between TiO₂ nanoparticles and CNTs. Fourier transform infrared spectroscopy (FTIR) spectra also present the evidence of CNTs interacting with TiO₂ nanoparticles (Fig. 3c).

Fig. 3d presents the XPS data of CNTs@TiO₂ nanohybrids. There are three peaks at around 297.5, 469.1 and 520.3 eV that correspond with C_{1s}, Ti_{2p}, and O_{1s} spectra, respectively. The XPS result additionally reveals that CNTs@TiO₂ nanohybrids have a Ti/O molar ratio of 0.46, indicating that CNTs also have some oxygen-containing groups on its surface, which can result from the annealing treatment or the residue carbonaceous polymer. According to EDX spectroscopy, the as-synthesized CNTs@TiO₂ nanohybrids are comprised of 48.5 wt.% Ti, 16.4 wt.% C, and 35.1 wt.% O, respectively.

The porous structure and the surface area of CNTs@TiO₂ nanohybrids were investigated through the nitrogen adsorption–desorption isotherm curves. The CNTs@TiO₂ nanohybrids exhibit a distinct hysteresis loop at the high relative pressure region; such a curve is a characteristic of different processes between adsorption into and desorption from mesopores (Fig. 3e). Based on the

nitrogen adsorption–desorption data, the CNTs@TiO₂ displays a Brunauer–Emmett–Teller (BET) surface area of 109.9 m² g⁻¹ and a pore volume of 0.18 cm³ g⁻¹, which are between the corresponding values for CNTs (160.6 m² g⁻¹ and 0.22 m³ g⁻¹) and for TiO₂ nanoparticles (53.7 m² g⁻¹ and 0.14 cm³ g⁻¹). Pore size distribution curves were plotted by using the Barrett–Joyner–Halenda (BJH) method. The CNTs@TiO₂ exhibits an average pore size of 11.5 nm (Fig. 3f), which was quite different from those of CNTs and TiO₂ nanoparticles (Supporting information, Fig. S4a–d). These results suggest that the overlaying of TiO₂ nanoparticles on CNTs did result in distinct changes in the total pore volume and the BET surface area.

To achieve fair evaluation of the anode effect in MFCs, an H-type MFC was set up to investigate the electricity generation by plunging different electrodes in the same anode chamber without direct contact; in this way the three electrodes can share the same cathode chamber to construct three MFCs, namely CNTs-MFC, TiO₂-MFC and CNTs@TiO₂-MFC, as schematically shown in Fig. 4a. The discharge behavior of the MFC was evaluated at an external resistance of 10 Ω by monitoring the variation of current density with time. Fig. 4b shows batch cycle tests on the three MFCs running under the same condition. It is revealed that the output current density was reproducible over multiple runs for all MFCs, indicating that the anodes had been stably colonized with functional bacteria after the start-up period of around three months. The profile of current generation was closely related to substrate supply; as a result, the replacement of the anode solution with fresh organics (acetate) resulted in a corresponding increase of current density, while the current dropped off when the organic substrates were completely consumed. Clearly, the CNTs@TiO₂-MFC generated the maximum current density (*I*_{max}) of 3.10 ± 0.03 A m⁻², much higher than those of the CNTs-MFC (1.77 ± 0.06 A m⁻²) and the TiO₂-MFC (1.69 ± 0.07 A m⁻²).

It should be noted that the CNTs@TiO₂-MFC, TiO₂-MFC, and CNTs-MFC were also operated separately with a *R*_{ex} loading of 1 Ω under the same condition by disconnecting the other two anodes (Supporting information, Fig. S5). It was revealed that the

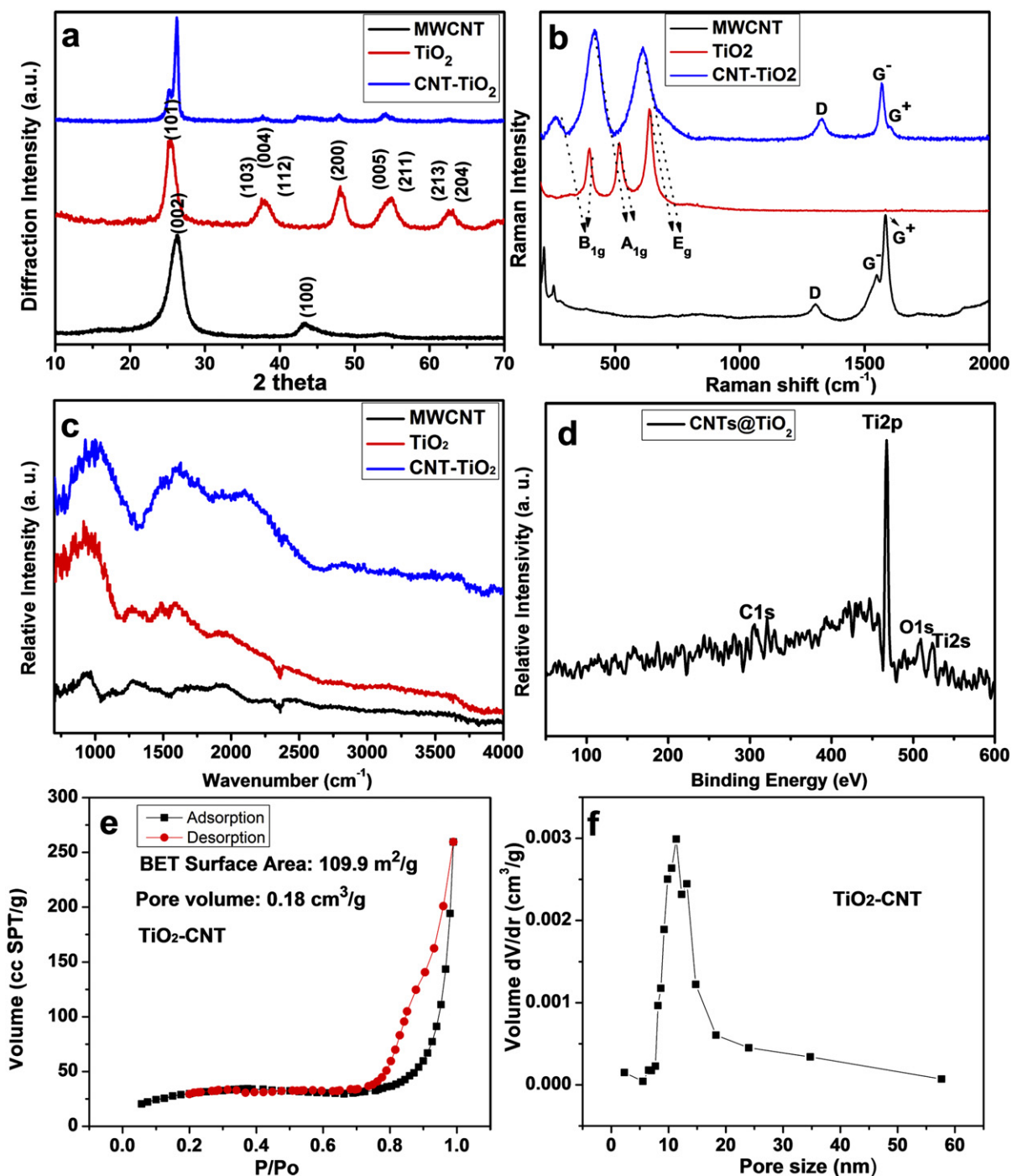


Fig. 3. XRD patterns (a), Raman spectra (b), and FTIR spectra (c) of CNTs, TiO₂ nanoparticles, and CNTs@TiO₂ hybrids; XPS spectrum (d), nitrogen adsorption/desorption isotherms (e) obtained at 77 K and pore size distribution (f) of the CNTs@TiO₂.

CNTs@TiO₂-MFC delivered a current density of 4.8 A cm⁻², much higher than those of TiO₂-MFC (2.7 A cm⁻²) and CNTs-MFC (3.0 A cm⁻²). This result was consistent with the above results when the three MFCs run simultaneously, demonstrating that there is no obvious influence among the three anode electrodes that shared a common cathode electrode. We also calculated the Coulombic efficiency (CE) of each MFC to illustrate the efficiency of organic-to-electricity generation based on the operation of individual MFCs [28,35]; it was found that the CNTs@TiO₂-MFC achieved a CE of 24.5%, about twice the corresponding CEs of the TiO₂-MFC (11.3%) and the CNT-MFC (12.7%).

The anode and cathode potentials were recorded versus the Ag/AgCl reference electrode during the polarization test. The three MFCs exhibited negligible difference in their cathode potentials because the same cathode was shared by all three anode electrodes (Supporting information, Fig. S6). The anode potentials, however, showed remarkable difference (Fig. 4c). When increasing the current density from 1.2 to 3.0 A cm⁻², the TiO₂ anode showed a drastic change from -0.38 V to -0.16 V in its potential, and the CNTs anode showed a moderate change from -0.42 V to -0.22 V, while the CNTs@TiO₂ anode had the least change from -0.54 V to -0.44 V, indicating a strong influence of the TiO₂ material on the anode

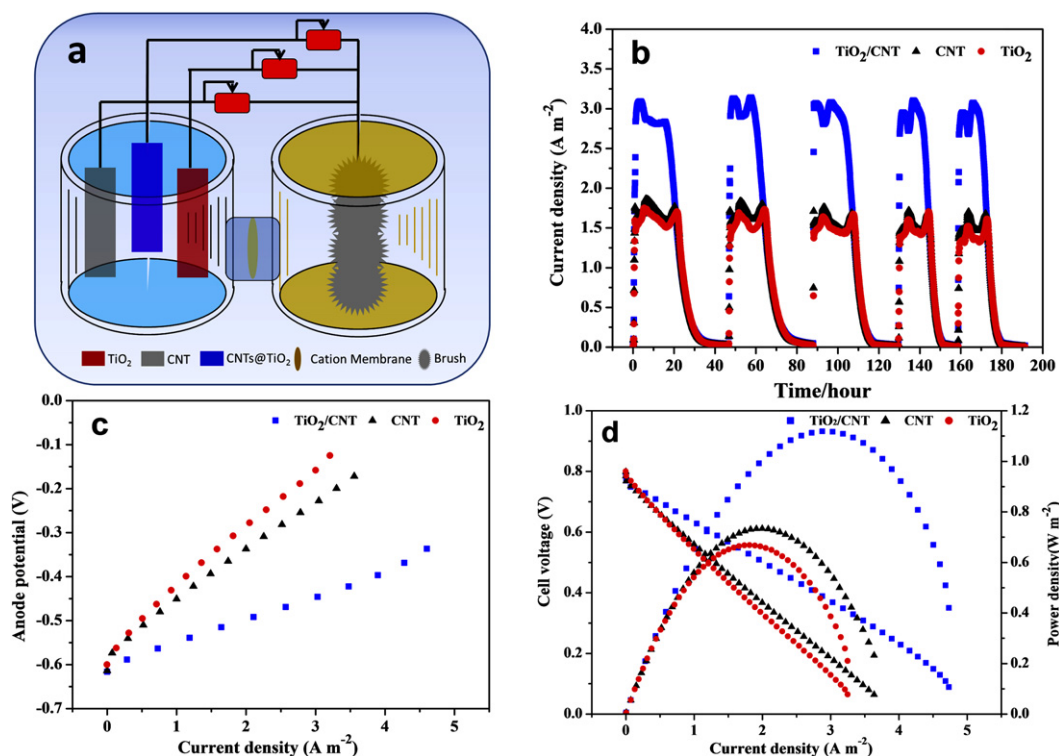


Fig. 4. (a) Schematic diagram of the designed MFC with three testing anodes in the anode chamber sharing the same cathode. (b) The output current vs. time at an R_{ex} loading of 10 Ω in CNTs-MFC, TiO₂-MFC, and CNTs@TiO₂-MFC. (c) Relation between current density and anode potential of the CNTs-MFC, TiO₂-MFC, and CNTs@TiO₂-MFC; and (d) MFC polarization and power density curves in CNTs-MFC, TiO₂-MFC, and CNTs@TiO₂-MFC. (Note: the power density was normalized based on the volume of the anode solution.)

potential. Obviously, a lower (more negative) anode potential benefits power production for fuel cell systems. The CNTs@TiO₂ anode kept the lowest potential among the three anode electrodes at the same current density, greatly favoring the electricity production. This result is in good agreement with results of batch tests and polarization curves.

Following the batch cycle test, the MFC performance was further evaluated by plotting the polarization and power density curves. Fig. 4d compares the polarization curves obtained from CNTs@TiO₂-MFC, TiO₂-MFC, and CNT-MFC, respectively. It was found that the three MFCs showed nearly the same V_{oc} of 0.79 ± 0.02 V, suggesting similar thermodynamics in all three MFCs. However, the CNTs@TiO₂-MFC attained an I_{max} of 4.73 A cm^{-2} , about 1.3 and 1.5 times of the I_{max} achieved by CNT-MFC (3.64 A cm^{-2}) and TiO₂-MFC (3.25 A cm^{-2}), respectively, indicating a stronger kinetic activity in the CNTs@TiO₂-MFC. Meanwhile, the TiO₂@CNTs-MFC produced a maximum power density of 1.12 W m^{-2} , about 1.5 and 1.7 times of those obtained with CNTs-MFC and TiO₂-MFC (0.73 W m^{-2} and 0.67 W m^{-2}), respectively.

To better understand the influence of the three anode materials on the MFCs, EIS experiments were conducted for all anodes at the open circuit potential, and the Nyquist plots are shown in Fig. 5. The resistance in the high frequency intercept of the real axis can be attributed to Ohmic resistance (R_{ohm}), which results from the electrode material, wire connection to the external circuit, and the electrolyte. The R_{ohm} values of the CNTs@TiO₂, TiO₂, and CNT anodes are approximately 8.97 Ω , 9.02 Ω , and 8.73 Ω , respectively, indicating that there was no distinct difference in the electrical conductivity of all three anodes. In the medium-to-low-frequency region, one unequal semicircle can be observed in the three anodes, with the diameter of the semicircle representing the charge-transfer resistance (R_{ct}) occurring at the anode. The Nyquist data was fitted with the equivalent circuit to calculate R_{ct} and double layer capacitance (C_{DL}) of the anode, as given in the inset of Fig. 5.

The R_{ct} of CNTs@TiO₂ anode was estimated to be 92 Ω , while the value for the CNT anode and the TiO₂ anode was 119 Ω and 142 Ω , respectively. Therefore, we can conclude that CNTs@TiO₂ nano-hybrids feature a lower charge-transfer resistance, signifying remarkable enhancement of the catalytic reaction and electron transfer in the CNTs@TiO₂ anode. Furthermore, the CNTs@TiO₂ displays a higher constant phase element (CPE, 0.97 μF) than that of CNTs (0.89 μF) and TiO₂ (0.81 μF), suggesting that bacteria can colonize well on the TiO₂/CNTs surface to produce a higher capacitance. The CNTs@TiO₂-MFC outperformed the CNT- and the TiO₂-based MFC in terms of various performance parameters, such as

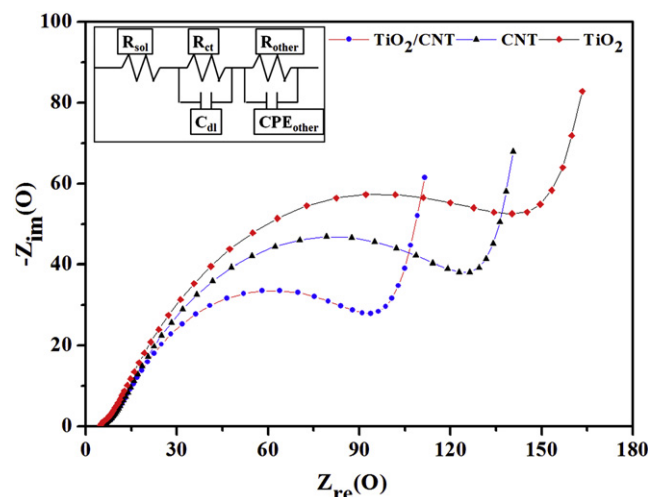


Fig. 5. Nyquist curves of the CNTs, TiO₂, CNTs@TiO₂ anodes in an MFC, respectively; inset is the corresponding equivalent circuit, note: R_{ct} is the charge-transfer resistance at the electrode interface; CPE is constant phase element; CDL is double layer capacitance of the anode.

maximum power density and Coulombic efficiency (Supporting information, Table S1).

According to the above results, the as-developed CNTs@TiO₂ nanohybrids have been proved to exhibit significantly improved electrochemical performance as anode materials for MFCs compared with TiO₂ nanoparticles and pure CNTs. Such an improvement can be reasonably attributed to the synergetic effect resulting from unique features of CNTs and TiO₂. On one hand, the CNTs@TiO₂ nanohybrids can well address the intrinsic issues of poor electrical conductivity and low porous structure associated with TiO₂ nanoparticles. The highly conductive CNTs core can significantly enhance the electrical conductivity, and the 1D structure with mesoporous structures can be beneficial to improve the mass transport of fuels and electrolytes, thus making favorable contributions to enhance output current density compared with TiO₂ nanoparticles. On the other hand, the CNTs@TiO₂ nanohybrids also exhibit favorable properties of good biocompatibility and large surface area, which facilitates the growth of anode-respiring microorganisms, resulting in increased catalytic activity or even lower overpotential to catalyze the fuel (acetate) oxidation.

4. Conclusion

In summary, we have demonstrated a facile and reliable route to synthesize nanohybrids of TiO₂ nanoparticles-decorating CNTs. The route to prepare CNTs@TiO₂ nanohybrids is very attractive because the CNTs@TiO₂ can be easily, economically, and effectively synthesized without using any surfactants and harsh environment. Moreover, the resulting CNTs@TiO₂ nanohybrids exhibit significantly improved performance as the anode electrode for an MFC compared with pure CNTs or TiO₂ nanoparticles. The superior electrochemical performance can be attributed to the synergetic effects between TiO₂ and CNTs due to their unique properties, such as relatively high surface area, good biocompatibility, improved electrical conductivity, excellent stability, and favorable surface functionalization for interfacial electrochemical reactions. Thanks to the possibility of facile synthesis and outstanding properties, the CNTs@TiO₂ may offer great potential for both fundamental study and industrial applications in catalysis, energy storage and conversion systems.

Acknowledgments

This work was financially supported by the U.S. National Science Foundation (ECCS-1001039 and CBET-1033505), the U.S. Department of Energy (DE-EE0003208), and the National Natural Science Foundation of China (No. 20903055 and No. 21206068).

Appendix A. Supplementary data

Supplementary data related to this article can be found at <http://dx.doi.org/10.1016/j.jpowsour.2013.01.146>.

References

- [1] B. Digman, D.S. Kim, *Environ. Prog.* 27 (2008) 524–537.
- [2] A.E. Franks, K.P. Nevin, *Energies* 3 (2010) 899–919.
- [3] B.E. Logan, B. Hamelers, R.A. Rozendal, U. Schröder, J. Keller, S. Freguia, P. Aelterman, W. Verstraete, K. Rabaey, *Environ. Sci. Technol.* 40 (2006) 5181–5192.
- [4] R.D. Cusick, Y. Kim, B.E. Logan, *Science* 335 (2012) 1474–1477.
- [5] A.A. Twite, S.C. Hsiao, H. Onoe, R.A. Mathies, M.B. Francis, *Adv. Mater.* 24 (2012) 2380–2385.
- [6] A. Rinaldi, B. Mecheri, V. Garavaglia, S. Licocchia, P. Di Nardo, E. Traversa, *Energy Environ. Sci.* 1 (2008) 417–429.
- [7] B.E. Logan, M. Elimelech, *Nature* 488 (2012) 313–319.
- [8] B.E. Logan, K. Rabaey, *Science* 337 (2012) 686–690.
- [9] R.C. Wagner, D.I. Call, B.E. Logan, *Environ. Sci. Technol.* 44 (2010) 6036–6041.
- [10] C.I. Torres, R. Krajmalnik-Brown, P. Parameswaran, A.K. Marcus, G. Wanger, Y.A. Gorby, B.E. Rittmann, *Environ. Sci. Technol.* 43 (2009) 9519–9524.
- [11] Y. Qiao, S.J. Bao, C.M. Li, *Energy Environ. Sci.* 3 (2010) 544–553.
- [12] M. Zhou, M. Chi, J. Luo, H. He, T. Jin, *J. Power Sources* 196 (2011) 4427–4435.
- [13] J.E. Mink, J.P. Rojas, B. Logan, M.M. Hussain, *Nano Lett.* 12 (2012) 791–795.
- [14] Y. Zhao, K. Watanabe, R. Nakamura, S. Mori, H. Liu, K. Ishii, K. Hashimoto, *Chem. Eur. J.* 16 (2010) 4982–4985.
- [15] B.E. Logan, S.A. Cheng, V. Watson, G. Estadt, *Environ. Sci. Technol.* 41 (2007) 3341–3346.
- [16] B.D. Alexander, P.J. Kulesza, L. Rutkowska, R. Solarska, J. Augustynski, *J. Mater. Chem.* 18 (2008) 2298–2303.
- [17] Q. Zhang, G. Cao, *Nano Today* 6 (2011) 91–109.
- [18] W. Smith, A. Wolcott, R.C. Fitzmorris, J.Z. Zhang, Y. Zhao, *J. Mater. Chem.* 21 (2011) 10792–10800.
- [19] G. Wang, H. Wang, Y. Ling, Y. Tang, X. Yang, R.C. Fitzmorris, C. Wang, J.Z. Zhang, Y. Li, *Nano Lett.* 11 (2011) 3026–3033.
- [20] H. Zhang, X. Lv, Y. Li, Y. Wang, J. Li, *ACS Nano* 4 (2010) 380–386.
- [21] Y. Qiao, S.J. Bao, C.M. Li, X.Q. Cui, Z.S. Lu, J. Guo, *ACS Nano* 2 (2008) 113–119.
- [22] Y. Qiao, C.M. Li, S.J. Bao, Q.L. Bao, *J. Power Sources* 170 (2007) 79–84.
- [23] T. Zhang, Y. Zeng, S. Chen, X. Ai, H. Yang, *Electrochem. Commun.* 9 (2007) 349–353.
- [24] A. Gomathi, S.R.C. Vivekchand, A. Govindaraj, C.N.R. Rao, *Adv. Mater.* 17 (2005) 2757–2761.
- [25] H.X. Zhang, C. Feng, Y.C. Zhai, K.L. Jiang, Q.Q. Li, S.S. Fan, *Adv. Mater.* 21 (2009) 2299–2304.
- [26] X. Chen, S.S. Mao, *Chem. Rev.* 107 (2007) 2891–2959.
- [27] D. Tasis, N. Tagmatarchis, A. Bianco, M. Prato, *Chem. Rev.* 106 (2006) 1105–1136.
- [28] S. Ci, Z. Wen, J. Chen, Z. He, *Electrochem. Commun.* 14 (2012) 71–74.
- [29] Z. Wen, S. Ci, F. Zhang, X. Feng, S. Cui, S. Mao, S. Luo, Z. He, J. Chen, *Adv. Mater.* 24 (2012) 1399–1404.
- [30] Z. Wen, Q. Wang, J. Li, *Adv. Funct. Mater.* 18 (2008) 959–964.
- [31] X. Sun, J. Liu, Y. Li, *Chem. Mater.* 18 (2006) 3486–3494.
- [32] M.M. Titirici, M. Antonietti, A. Thomas, *Chem. Mater.* 18 (2006) 3808–3812.
- [33] L. Shen, X. Zhang, H. Li, C. Yuan, G. Cao, *J. Phys. Chem. Lett.* 2 (2011) 3096–3101.
- [34] R. Kumar, S.B. Cronin, *Phys. Rev. B* 75 (2007) 155421.
- [35] H. Dong, H. Yu, X. Wang, *Environ. Sci. Technol.* 46 (2012) 13009–13015.